NEUROSCIENCE

Reward ameliorates depressive-like behaviors via inhibition of the substantia innominata to the lateral habenula projection

Yuting Cui[1,2]†, Xiaodan Huang[3,4]†, Pengcheng Huang[1,2]†, Lu Huang[3,4]†, Zhao Feng[5], Xinkuan Xiang[1,2], Xinfeng Chen[1,2], Anan Li[1,2,5], Chaoran Ren[3,6,7,8]*, Haohong Li[9,10]*

The lateral habenula (LHb) is implicated in emotional processing, especially depression. Recent studies indicate that the basal forebrain (BF) transmits reward or aversive signals to the LHb. However, the contribution of the BF-LHb circuit to the pathophysiology of depression still needs to be determined. Here, we find that the excitatory projection to the LHb from the substantia innominata (SI), a BF subregion, is activated by aversive stimuli and inhibited by reward stimuli. Furthermore, chronic activation of the SI-LHb circuit is sufficient to induce depressive-like behaviors, whereas inhibition of the circuit alleviates chronic stress–induced depressive-like phenotype. We also find that reward consumption buffers depressive-like behaviors induced by chronic activation of the SI-LHb circuit. In summary, we systematically define the function and mechanism of the SI-LHb circuit in modulating depressive-like behaviors, thus providing important insights to better decipher LHb processing in the pathophysiology of depression.

INTRODUCTION

Major depressive disorder is one of the most prevalent mood disorders that can occur for a variety of reasons related to genetics, illness, or the environment (*1*). Chronic uncontrollable aversive stimulation (AS) can lead to various pathologies, including psychological dysfunctions such as depression (*2*, *3*). Many studies support the antidepressive effects of cognitive, pharmacological, and light therapies (*4*–*7*). In addition, reward food or increased reward experience has been considered as a strategy to alleviate negative/depressive emotions in humans (*8*, *9*). In rodents, previous studies have demonstrated that palatable food intake (or sugar drink) for a few days is sufficient to dampen behavioral responses to stress induced by acute or chronic stress (*10*, *11*). These imply that reward can resist behavioral responses to negative stimuli across species (*12*, *13*).

The lateral habenula (LHb), a brain region implicated in depression, encodes numerous stimuli, including reward, reward omission, and punishment, and it is centrally positioned to transform emotional information into proper behaviors, particularly in response to stress (*14*–*21*). Unexpected nonrewarding or unpleasant events can activate LHb neurons, while reward delivery can conversely decrease the LHb neuronal activity (*14*). In addition, acute stress transforms the reward signal encoded by the LHb into punishment-like neural signals, which may contribute to depression (*22*). An elegant set of experiments showed that reducing hyperactivity of the LHb can ameliorate depressive symptoms (*15*, *23*, *24*). Furthermore, loss of function in the LHb of animal models impairs learning ability, particularly to aversive stimuli in avoidance tasks (*25*, *26*). These suggest that hyperactivity of the LHb neurons may serve as a neural mechanism to facilitate stress-induced emotional disorders. The LHb receives inputs from several forebrain limbic circuits involved in emotion processing and sends outputs to the midbrain circuits involved in motivation, reward, motor, and cognitive functions (*27*–*29*). The limbic and basal ganglia structures, such as the globus pallidus, lateral hypothalamic area, basal forebrain (BF), and paraventricular nucleus inputs also innervate the LHb (*30*–*33*). Among the upstream regions of the LHb, inputs from BF are widely implicated in processing punishment and reward signals (*34*, *35*). Cholinergic, glutamatergic, and GABAergic neurons are three major cell types spatially intermingled in the BF (*36*). The lateral preoptic area (LPO), as the major input from the BF to the LHb, exerts bivalent control over the LHb (*37*, *38*). Both LPO-glutamatergic and LPO-GABAergic inputs to the LHb are activated by aversive stimuli and their predictive cues yet produce opposing behaviors when stimulated independently (*38*). Ventral pallidum (VP), another subregion of BF, also mediates reward and aversion implicated in depression via projecting to the LHb (*31*). Substantia innominata (SI) (fig. S1E), a subregion of the BF and close to the VP, which has also been classified as the extended amygdala, projects to the LHb, and the dorsal part of the posterior SI also receives dense inputs from the central amygdala, a major region of processing aversive emotions (*37*, *39*). Similar to other subregions of the BF, the SI exhibits considerable cellular heterogeneity and is implicated in neuropsychiatric disorders (*40*). Our earlier work reported that selective activation of SI glutamatergic neurons induces real-time conditioned place aversion (CPA), whereas activation of GABAergic neurons induces real-time conditioned place preference (CPP) (*39*). However, it is still unknown how strong each type of neuron from the SI forms synaptic connectivity

[1]Britton Chance Center for Biomedical Photonics, Wuhan National Laboratory for Optoelectronics, Huazhong University of Science and Technology, Wuhan, Hubei 430074, China. [2]MoE Key Laboratory for Biomedical Photonics, Collaborative Innovation Center for Biomedical Engineering, School of Engineering Sciences, Huazhong University of Science and Technology, Wuhan, China. [3]Guangdong-Hongkong-Macau Institute of CNS Regeneration, Ministry of Education CNS Regeneration Collaborative Joint Laboratory, Jinan University, Guangzhou 510632, China. [4]Department of Neurology and Stroke Center, The First Affiliated Hospital of Jinan University, Guangzhou 510632, China. [5]HUST-Suzhou Institute for Brainsmatics, JITRI Institute for Brainsmatics, Suzhou, China. [6]Bioland Laboratory (Guangzhou Regenerative Medicine and Health Guangdong Laboratory), Guangzhou 510530, China. [7]Center for Brain Science and Brain-Inspired Intelligence, Guangdong-Hong Kong-Macao Greater Bay Area, Guangzhou 510515, China. [8]Co-innovation Center of Neuroregeneration, Nantong University, Nantong 226001, China. [9]Affiliated Mental Health Centre and Hangzhou Seventh People's Hospital, Zhejiang University School of Medicine, Hangzhou, 310013 Zhejiang, China. [10]The MOE Frontier Research Center of Brain and Brain-Machine Integration, Zhejiang University School of Brain Science and Brain Medicine, Hangzhou 310058, China.
*Corresponding author. Email: hhli_27@zju.edu.cn (H.L.); tchaoran@jnu.edu.cn (C.R.)
†These authors contributed equally to this work.

with the LHb and how the SI instructs LHb neurons to encode aversive and reward stimuli and modulates mental disorders.

Here, electrophysiological recordings confirmed that the SI preferentially transmits glutamatergic inputs to LHb neurons. Fiber photometry revealed that SI excitatory inputs in the LHb are rapidly and strongly excited by aversive stimuli and inhibited by reward consumption. Using in vivo multichannel recordings, we observed that SI glutamatergic inputs are necessary for LHb neurons encoding aversive stimuli. Combining depressive-like behavioral tasks in male mice with chemogenetics showed that the glutamatergic SI-LHb circuit modulates depressive-like behaviors by changing the LHb neuronal excitability. We found that reward ameliorates depressive-like behavior induced by activation of the glutamatergic SI-LHb circuit. Together, our findings systematically defined the function of the SI-LHb circuit mediating depressive-like behaviors.

RESULTS

The opposite responses of the SI_{VGluT2}-LHb neural circuit to aversive and reward stimuli

We first elaborated the anatomical and functional relationship of the SI and the LHb using anterograde viral tracing and electrophysiology. Anterograde virus AAV-hSyn-DIO-EGFP (enhanced green fluorescent protein) was injected into the SI of the Vglut2-ires-Cre mice/Vgat-ires-Cre mice for labeling glutamatergic/GABAergic neural output fibers with EGFP. Brains were sliced and imaged using confocal microscopy after 21 days of virus expression. Meanwhile, we also combined anterograde adeno-associated virus (AAV) tracing of SI glutamatergic neurons and fluorescence micro-optical sectioning tomography (fMOST) with whole-brain imaging (fig. S1E). To determine whether we can specifically target the SI, we quantified EGFP-labeled neurons in SI, VP, and LPO in Vglut2-ires-Cre mice, which account for 85.68, 7.72, and 6.60% of the total counted neurons in the virus injection site, respectively (fig. S1A). The results suggested that the brain region we targeted predominantly resides in the SI. Outputs (axon projections) of the SI neuron to multiple brain regions were quantified as the ratio of the pixels occupied by detected EGFP axons. Relatively dense fluorescence expression was observed in six major downstream brain regions (fig. S1, B to D). Among these subdivisions, the LHb and stria medullaris (SM) received stronger SI glutamatergic projections, while the medial habenular nucleus, substantia nigra, ventral tegmental area (VTA), and pedunculopontine tegmental nucleus (PPTg) received less SI inputs (fig. S1, B, C, and F). SI GABAergic neurons also project to LHb, VTA, and PPTg (fig. S1, C and D). As the SM is usually considered to be a fiber bundle containing afferent fibers from regions other than the habenula (*41*), LHb is the major downstream target of SI neurons (fig. S1, C and F). To further explore the functional relationship of SI-LHb projections, we injected virus AAV-CAG-ChR2-GFP expressing the light-activated ion channel channelrhodopsin-2 (ChR2) into the SI of C57BL/6J mice and recorded postsynaptic currents in LHb neurons by optogenetically activating SI-LHb projections (fig. S2A). Exclusive excitatory postsynaptic currents (EPSCs) were observed in 48.9% of recorded neurons, whereas 6.7% of recorded neurons only received inhibitory inputs, with a mix of both inhibitory postsynaptic currents (IPSCs) and EPSCs detected in 24.4% of recorded neurons (fig. S2B). Furthermore, the EPSCs in response to SI-LHb activation could be blocked by the AMPA receptor antagonist 6-cyano-7-nitroquinoxaline-2,3-dione (CNQX), while IPSCs could be blocked by the γ-aminobutyric acid type A ($GABA_A$) receptor antagonist picrotoxin (PTX) (fig. S2C). Last, light-evoked postsynaptic currents in the LHb neurons were completely blocked by the application of sodium blocker [tetrodotoxin (TTX)] and restored by coapplication of TTX and potassium channel blocker 4-AP (4-aminopyridine), confirming that LHb neurons received monosynaptic inputs from SI neurons (fig. S2D). Therefore, these results provide direct evidence that the SI predominately transmits excitatory inputs to LHb neurons via monosynaptic connections.

The LHb activity can be modulated by aversive and reward stimuli (*14*, *20*). To confirm the response of the SI_{VGluT2}-LHb neural circuit to different stimuli, we recorded Ca^{2+} transients of SI_{VGluT2}-LHb terminals using fiber photometry when aversive or rewarding stimuli were delivered (Fig. 1A) (*42*, *43*). A Cre-dependent AAV encoding the Ca^{2+} indicator GCaMP6m (AAV-EF1α-DIO-GCaMP6m) and a control virus (AAV-hSyn-DIO-EGFP) were separately injected into the SI of Vglut2-ires-Cre mice (Fig. 1B). We also injected virus AAV-EF1α-DIO-GCaMP6m mixed with AAV-CAG-Flex-mCherry (1:1) into the SI of Vglut2-ires-Cre mice to simultaneously monitor signals in the GCaMP channel and the within-subject control mCherry channel (fig. S3, E and F). An optical fiber was implanted above the LHb (Fig. 1, B and C, and fig. S6, A and D). Footshock (0.5 mA, 0.2 s), air puff (0.2 MPa, 0.2 s), water (15 μl in 0.2 s), sucrose [5% (w/v), 15 μl in 0.2 s], and chocolate (0.1 g) were delivered, respectively. We found that aversive stimuli reliably elicited obvious Ca^{2+} transient increase in the SI_{VGluT2}-LHb terminals (Fig. 1, D, E, and K, and fig. S3G). However, when mice voluntarily received water or sweet solution by licking a nozzle, GCaMP6m fluorescence of the SI_{VGluT2}-LHb terminals was significantly decreased (Fig. 1, F, G, and K). Stimuli-evoked responses were not observed in EGFP-expressing control mice (fig. S3, A to D). In free-moving mice, SI_{VGluT2}-LHb activity was also inhibited upon solid chocolate consumption (Fig. 1, H and K, and fig. S3H). Meanwhile, aversive and reward-evoked responses were not observed in the control mCherry channel (fig. S3, G and H). These results demonstrate that the SI_{VGluT2}-LHb circuit can be bidirectionally modulated by aversive and reward stimuli. A recent study reported that acute stress transforms LHb responses to reward into punishment-like neural signals (*22*). Considering that aversive stimuli can activate and reward can inhibit the activity of the SI_{VGluT2}-LHb circuit, we asked whether reward consumption could influence the responses of the SI_{VGluT2}-LHb circuit to aversive stimuli. Notably, although reward (sucrose or liquid chocolate) delivery accompanying air puff instantaneously increased GCaMP6m fluorescence, the response intensity of the SI_{VGluT2}-LHb circuit to aversive stimuli was subsequently abolished and transformed into the reward-like response (Fig. 1, I, J, and L). It seems that reward signals encoded by the SI_{VGluT2}-LHb circuit suppressed aversive signals, indicating that reward consumption might alleviate the response of mice to aversive stimuli by inhibiting the activity of the SI_{VGluT2}-LHb circuit.

SI excitatory inputs are required for LHb to encode aversive signals

LHb neurons can be activated by aversive stimuli, which may be a neural mechanism to facilitate stress-induced emotional disorders. We next test whether SI glutamatergic neurons contribute to aversive stimulus–mediated LHb single-cell dynamics using chronic in vivo single-unit recording. $VGluT2^+$ neurons on one side of the SI were

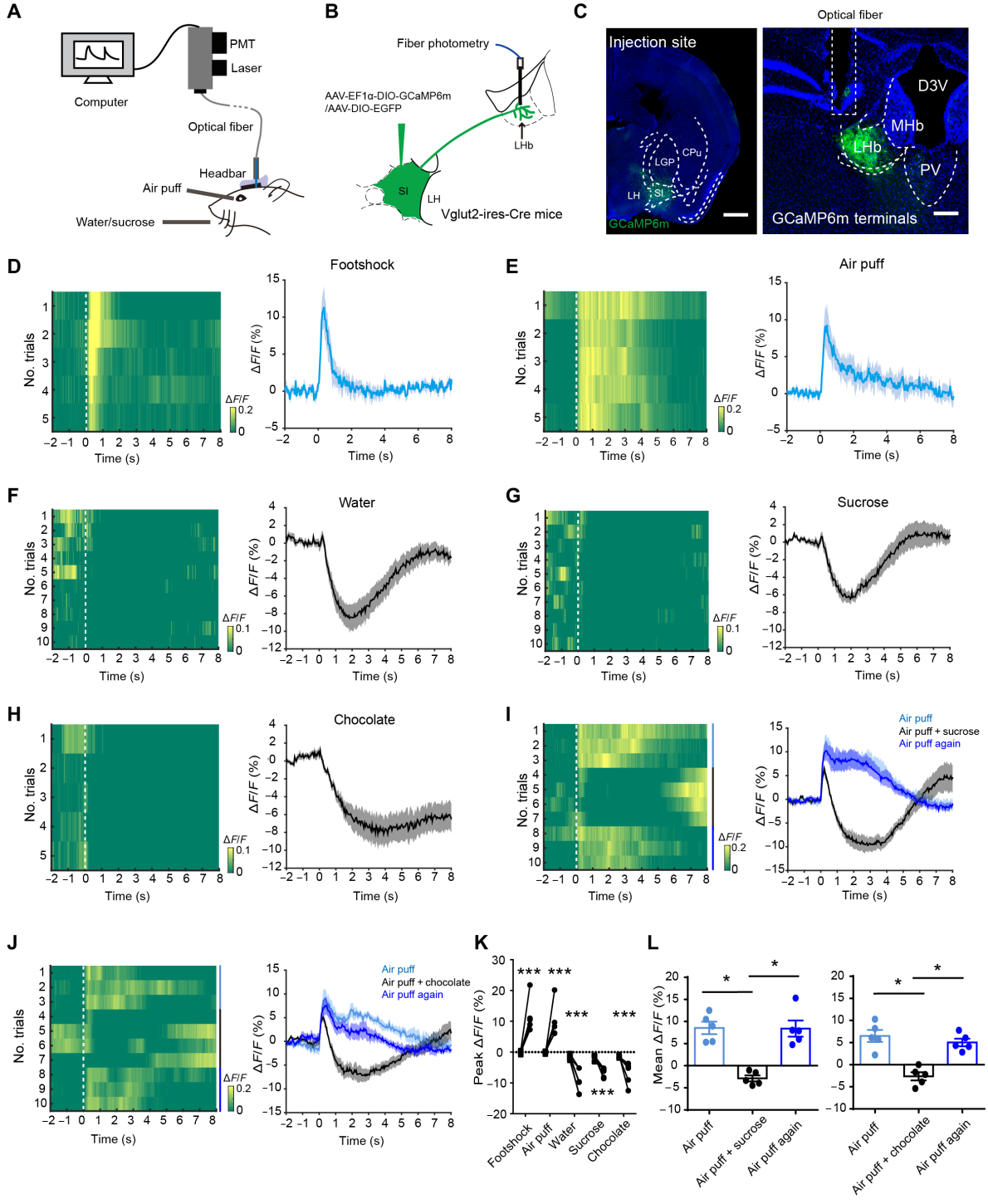

Fig. 1. Reward impairs aversive stimuli–induced activation of the SI_{VGluT2}-LHb neural circuit. (**A**) Setup of the fiber photometry system for head-fixed mice. (**B**) Schematic diagram of virus injection and implanted fiber in Vglut2-ires-Cre mice. (**C**) Images show the virus injection site (scale bar, 1 mm) and optic fiber position in LHb. LH, lateral hypothalamus; CPu, caudate putamen; LGP, lateral globus pallidus. Scale bar, 200 μm. (**D** to **H**) Left: Representative heatmap of Ca^{2+} signals (bottom left) from a mouse aligned to the initiation of footshock (0.5 mA, 0.2 s), air puff (0.2 MPa, 0.2 s), water (15 μl), sucrose (5%, 15 μl), and chocolate (0.1 g). Color scales on the right indicate Δ*F*/*F*. Right: Mean Ca^{2+} transients aligned to events starting with stimuli (footshock: $n = 5$; air puff: $n = 5$; water: $n = 6$; sucrose: $n = 6$; chocolate: $n = 6$). Data are means ± SEM. (**I** and **J**) Left: Heatmap of Ca^{2+} signals (bottom left) from a mouse aligned to three continuous sessions: air puff, air puff + sucrose/liquid chocolate, and air puff again. Right: Averaged calcium signals from three sessions. $N = 5$ mice. (**K**) Comparison of peak Δ*F*/*F* between baseline (4 s before stimuli) and stimuli (within 5 s from onset of stimuli) of the SI_{VGluT2}-LHb circuit in response to different stimuli. Paired two-tailed *t* test: ***$P < 0.001$. (**L**) Quantification of changes in calcium signals from three sessions: air puff, air puff + sucrose/liquid chocolate, and air puff again. One-way analysis of variance (ANOVA) with Bonferroni multiple comparisons test, air puff versus air puff + sucrose: *$P = 0.01$, air puff + sucrose versus air puff again: *$P = 0.03$; air puff versus air puff + chocolate: *$P = 0.03$, air puff + sucrose versus air puff again: *$P = 0.03$. Data are means ± SEM.

ablated by injecting AAV-DIO-tasCasp3-TEVp into the SI of Vglut2-ires-Cre mice to avoid functional compensation of contralateral projections in the LHb. On the other side of the SI, we inhibited the SI_{VGluT2}-LHb circuit with Cre-inducible archaerhodopsin (ArchT), which is a light-sensitive inhibitory proton pump (Fig. 2B). A 125-μm optical fiber and 16-microwire bundle were implanted into the LHb side expressing ArchT for light delivery and recording, respectively (Fig. 2B). The mouse is head-fixed, and air puff (0.2 MPa, 0.5 s) is delivered to the eye (Fig. 2A). The injection site, electrode placements, and ArchT-expressing terminals (green) were observed (Fig. 2C and fig. S6, B and E). Consistent with the results of the fiber photometry, air puff led to a rapid increase in action potentials in 34.65% (44 of 127) of neurons recorded across the LHb (Fig. 2, D to G). To test whether SI glutamatergic neurons contribute to aversive stimulus–evoked LHb single-cell dynamics, we recorded the activity of the LHb neurons in response to air puff while a 532-nm laser was delivered for inhibiting SI excitatory inputs in 50% of trials. We found that the neuronal firing was significantly attenuated in 43.18% (19 of 44) of neurons evoked by air puff when SI excitatory inputs were optogenetically inhibited, and only 22.73% (10 of 44) of neurons were potentiated (Fig. 2, H to J). Optogenetic inhibition of SI excitatory inputs did not obviously affect the LHb neural spontaneous activity (fig. S4). These results indicated that most LHb neurons in response to aversive stimuli were regulated by SI excitatory inputs.

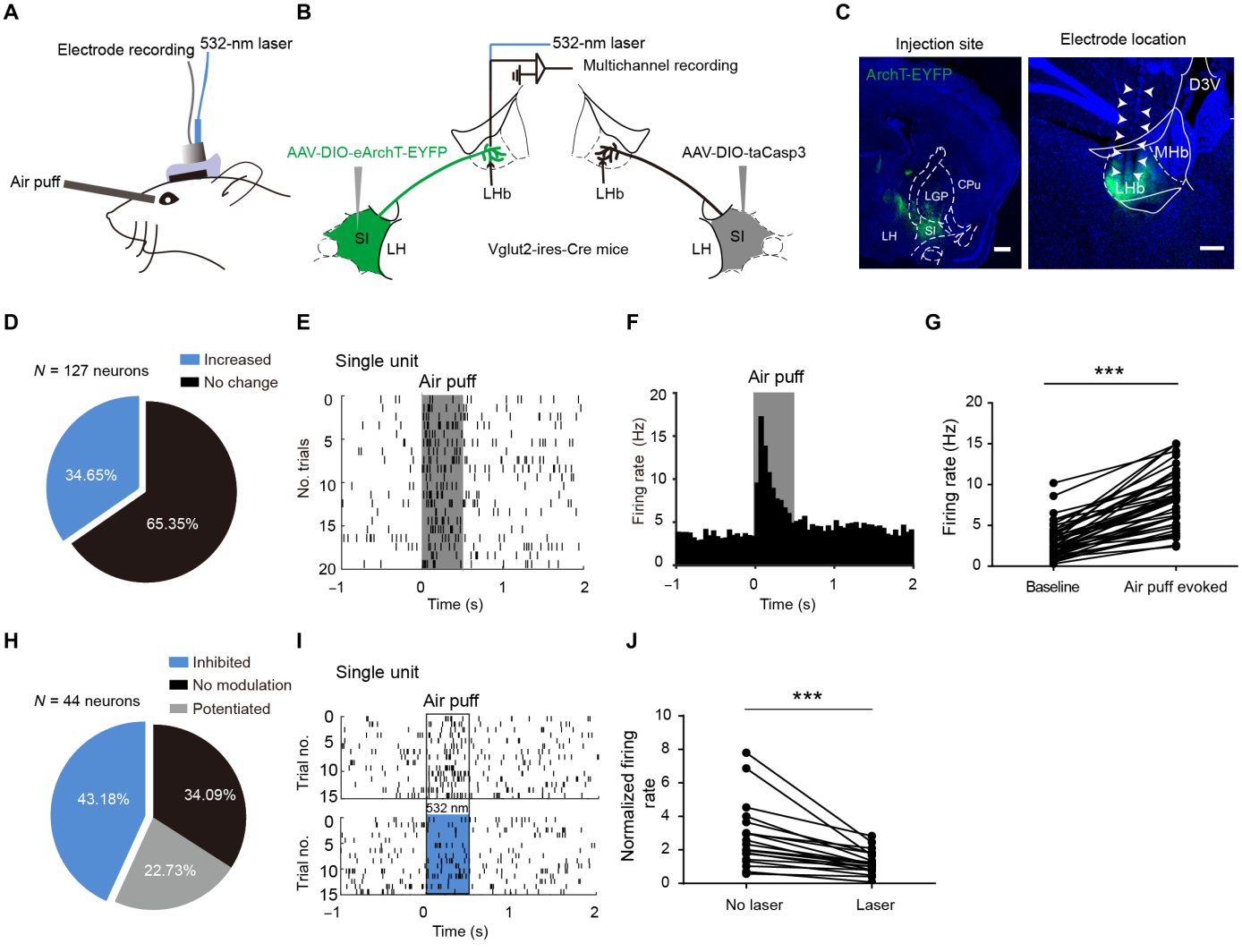

Fig. 2. Inhibition of the SI excitability inputs reduces LHb response to aversive stimuli. (**A**) Virus injection and the electrode placement for selective inhibition of SI_{VGluT2}-LHb neural circuit. (**B**) Schematic diagram placement of virus injection and multichannel recording in Vglut2-ires-Cre mice. (**C**) Anatomical image in the SI showing virus injection site (scale bar, 500 μm) and anatomical image in the LHb showing electrode traces. Scale bar, 100 μm. ArchT-expressing (green) terminals were observed in the LHb. (**D**) Cells (34.65%) increased firing rates modulated by air puff. $N = 4$ mice. (**E**) Raster of an example LHb neuron in response to the air puff. (**F**) Meaning of firing rate in population neurons ($n = 44$) in response to air puff. Bin = 50 ms. (**G**) Mean spikes of population neurons ($n = 44$) in response to air puff (0.5 s). Paired t test, $^{***}P < 0.001$. Each dot represents one cell. (**H**) Cells (43.18%) decreased firing rates induced by air puff compared with no 532-nm laser delivered. (**I**) Representative air puff–evoked spike raster plot in a single neuron with a 532-nm laser or not. (**J**) Mean-normalized firing rate of population neurons in response to air puff with a 532-nm laser or not ($n = 19$). Paired t test, $^{***}P < 0.001$.

Activation of the SI_{VGluT2}-LHb circuit induces aversive behaviors

Activation of glutamatergic neurons in the SI can induce CPA, and activation of GABAergic neurons can drive CPP (*39*). To determine the behavioral consequences of activating SI inputs to the LHb, we injected the AAV virus expressing Cre-inducible ChR2 virus AAV-DIO-ChR2-EYFP or control virus (AAV-DIO-EGFP) into the LHb of Vglut2-ires-Cre mice (Fig. 3B and fig. S6F). Optical fibers were implanted above the LHb to shed light on SI glutamatergic axonal fibers (Fig. 3, A and B, and fig. S6C). Mice were tested in the real-time place preference (RTPP) assay (Fig. 3C). Photostimulation (10-ms pulse at 30 Hz) was continuously delivered when mice entered one chosen chamber and terminated when the mice exited this chamber. The SI_{VGluT2}-LHb^{ChR2} mice displayed avoidance of the photostimulation-paired chamber and spent significantly more time in the photostimulation-unpaired chamber (Fig. 3, D and E). Activation of the SI_{Vglut2}-LHb circuit did not obviously affect the locomotor activity of mice, as demonstrated by the comparable total distance and mean speed (fig. S9A). Considering that SI GABAergic neurons also project to the LHb (fig. S1), we also tested the behavioral effects of the SI_{GABA}-LHb circuit using the same strategy (fig. S5A). Mice did not show any preference for either side of the chamber while the SI_{GABA}-LHb circuit was activated (fig. S5, B and C).

In addition, we also monitored licking suppression behavior in water-deprived head-fixed mice when the SI_{VGluT2}-LHb circuit was activated (Fig. 3, F and H) (*44*, *45*). Considering that activation of the SI_{VGluT2}-LHb circuit induces CPA, we speculated that activation of the SI_{VGluT2}-LHb circuit might decrease ongoing licking behavior by transmitting aversive signals. A 473-nm laser for activating the SI_{VGluT2}-LHb circuit was delivered randomly while mice licked water (Fig. 3, F and H). In laser delivery trials, photostimulation elicited obvious suppression of licking, as indicated by the lower speed and higher licking suppression index (Fig. 3, G, I, and J). However, this was reversed upon the cessation of light, as shown by quantification of the effects of laser delivery on licking behavior (Fig. 3, G, I, and J). The licking behavior in the control group was not affected by the laser (Fig. 3, G, I, and J). In summary, activation of this circuit can have aversive effects and suppress reward consumption.

SI_{VGluT2}-LHb circuit modulates depressive-like behaviors

Many studies have shown that direct optogenetic activation or increased LHb neuronal activity induced by long-term exposure to chronic uncontrollable AS can lead to depressive-like behaviors (*17*, *19*, *21*). Given that glutamatergic SI inputs contribute to LHb neuron processing an aversive signal (Fig. 2), we first investigated whether the aversive signal induced by chronic activation of the SI_{VGluT2}-LHb circuit was sufficient to induce depressive-like behaviors. Using the dual-virus strategy, we injected retrogradely transported and Cre recombinase–dependent AAV-Retro-DIO-flp into the LHb and injected Flp-dependent AAV-hSyn-fDIO-hM3D-mCherry into the SI of Vglut2-ires-Cre mice, which allows specifically activating LHb-projecting SI neurons (Fig. 4, A and B, and fig. S6G). Efficacy of chemogenetic activation was confirmed by in vitro patch-clamp recording (fig. S7). Clozapine-*N*-oxide (CNO) treatment induced depolarization of the resting membrane potential in SI neurons expressing hM3D (fig. S7A), showing that the activity of the hM3D-expressing SI neurons could be regulated by CNO. To test whether CNO administration by itself can affect the behaviors, we also injected AAV-Retro-DIO-flp into the LHb and AAV-hE-F1a-fDIO-mCherry as an empty vector control into the SI of Vglut2-ires-Cre mice (fig. S8A). After virus expression for 14 days, for the hM3D-CNO group, CNO (2 mg/kg) was intraperitoneally injected into mice daily to activate the SI_{VGluT2}-LHb pathway for 14 days (Fig. 4C and fig. S8B). For the hM3D-saline control group, saline was injected into mice daily (Fig. 4C). Then, mice were subjected to a series of depression- and anxiety-related behavioral tests. Long-term activation of the SI_{VGluT2}-LHb pathway significantly increased the depressive-like behaviors tested in the sucrose preference test (SPT), forced swimming test (FST), and novelty-suppressed feeding test (NSF), and the anxiety level was significantly elevated in the open-field test (OFT) but not in the elevated plus-maze test (EPM) (Fig. 4, D and E). Locomotor activity, measured by total distance traveled in OFT, showed no obvious difference in both groups (fig. S9B). Meanwhile, CNO administration by itself could not affect depressive-like behaviors induced by chronic activation of the SI-LHb circuit (fig. S8, C and D). These results are consistent with a previous study about the LHb modulating typical anxiety-like behaviors induced by exposure to inescapable tail shock or chronic stress (*46*). Aberrant LHb neuronal activity is closely associated with depression (*21*, *47*, *48*). This prompted us to further explore the LHb neuronal activity after chronic activation of the SI_{VGluT2}-LHb circuit. We test the LHb neural excitability without the glutamate/GABA blockers and found that LHb neurons from mice with long-term activation of the SI_{VGluT2}-LHb circuit fired more action potentials in response to current injections (Fig. 4F), indicating that long-term activation of SI excitatory inputs increased the excitability of LHb neurons, which may be the underlying mechanism for elevated depressive- and anxiety-like behaviors.

To determine whether the activity of the SI_{VGluT2}-LHb pathway was necessary for depressive symptom formation, we inhibited the activity of the SI_{VGluT2}-LHb pathway during the chronic mild stress model (CMS). AAV-Retro-DIO-Flp was injected into the bilateral LHb and AAV-hSyn-fDIO-hM4D(Gi)-mCherry was injected into the SI of Vglut2-ires-Cre mice (Fig. 4G and fig. S6H). After 14 days of virus expression, patch-clamp recording first confirmed that CNO treatment could induce hyperpolarization of the resting membrane potential in neurons expressing hM4Di (fig. S7B), showing that the activity of hM4Di-expressing SI neurons could be regulated by CNO. Mice were divided into three groups: hM4D-CMS-CNO, hM4D-CMS-Saline, and hM4D-control groups. For the hM4D-CMS-CNO group, the SI_{VGluT2}-LHb pathway was inhibited daily via intraperitoneal injection of CNO 30 min before mice were treated with AS (footshock, 20 times/day; air puff, 20 times/day; fox urine, 30 min/day; physical restraint, 1 hour/day) for 28 days. For the hM4D-CMS-Saline group, mice were treated with the same AS for 28 days and a daily intraperitoneal injection of saline 30 min before AS (Fig. 4H). For the hM4D-control group, mice only went through the same environment as with the CMS group daily. First, after long-term exposure to AS, hM4D-CMS-Saline mice exhibited increased depressive- and anxiety-like behaviors, as tested by the SPT, FST, NSF, and OFT, compared with the hM4D-control group (Fig. 4, I and J), accompanied by significantly increased LHb excitability (Fig. 4K). Comparing the hM4D-CMS-CNO group with the hM4D-CMS-Saline group, we found that inhibition of the SI_{VGluT2}-LHb pathway alleviated the depressive-like behaviors induced by long-term exposure to AS, although the NSF and OFT anxiety-like behaviors were not significantly altered (Fig. 4, I and J). Locomotor activity did not differ between the

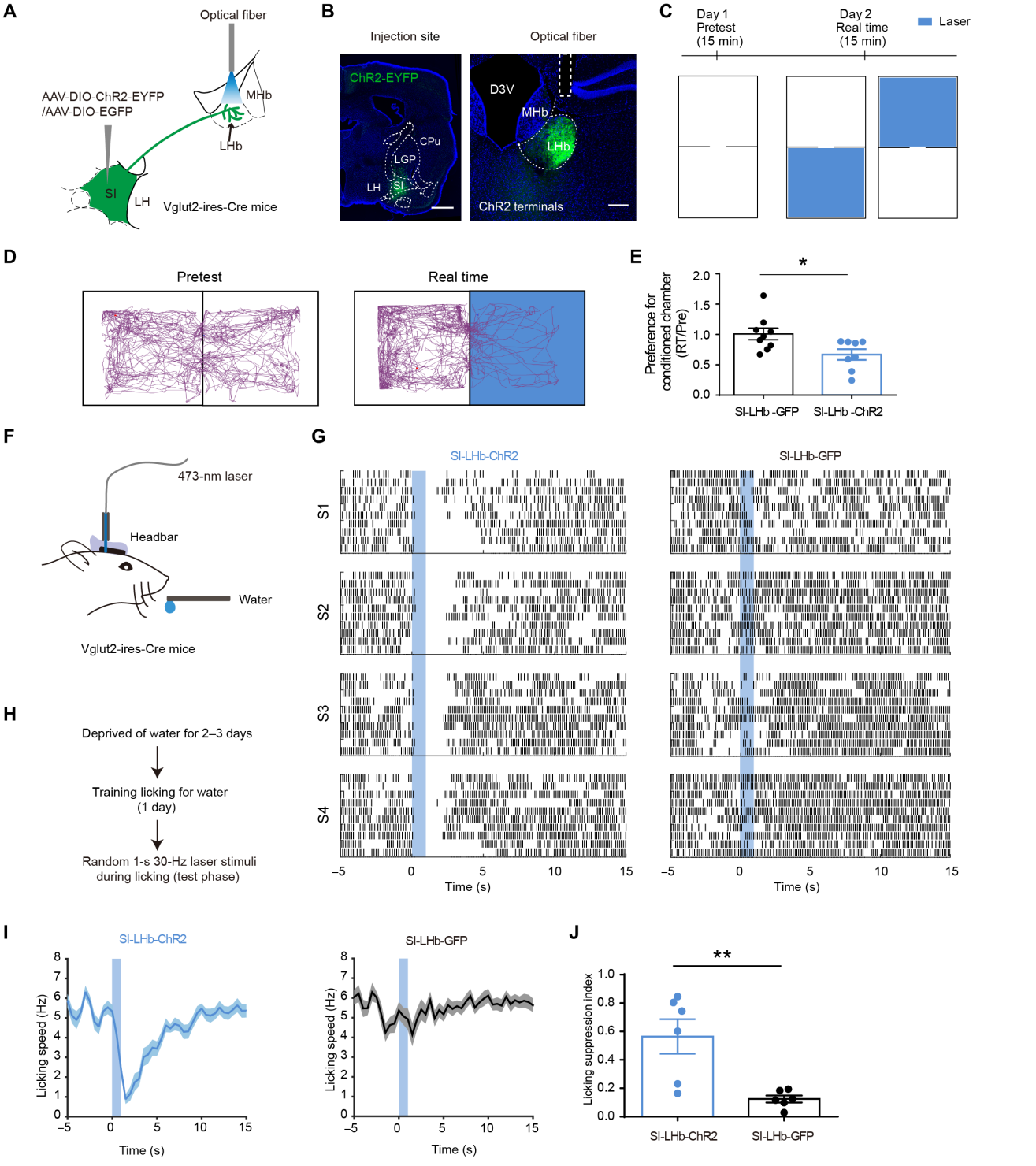

Fig. 3. Activation of the SI_{VGluT2}-LHb neural circuit induces aversive-like behaviors. (**A**) Virus injection and optical fiber placement for selective activation of the SI-LHb neural circuit. (**B**) Images show the ChR2 virus injection site in the SI (scale bar, 1 mm) and implanted site of optical fiber in the LHb. Scale bar, 200 μm. (**C**) Procedure for RTPP performance. (**D**) Examples of pretest and real-time behavior trace accompanying photostimulation of the SI_{VGluT2}-LHb neural circuit. (**E**) Aversion or preference for a place where the SI_{VGluT2}-LHb neural circuit was activated. Unpaired *t* test, preference for conditioned chamber: $^{*}P = 0.02$. Data are means ± SEM. (**F**) Schematic of the head-fixed experimental configuration of the lick suppression task. (**G**) Representative licking raster in response to laser stimuli (1 s, 30 Hz, 10 ms) from a ChR2-expressing mouse and a GFP-expressing mouse in four sessions. (**H**) Timeline of the experimental procedure in the lick suppression task. (**I**) Average speed of licking from ChR2-expressing and GFP-expressing mice is shown. (**J**) Average suppression index in response to laser stimuli. ChR2: $n = 6$ mice; GFP: $n = 6$ mice, unpaired *t* test, $^{**}P = 0.005$. Data are means ± SEM.

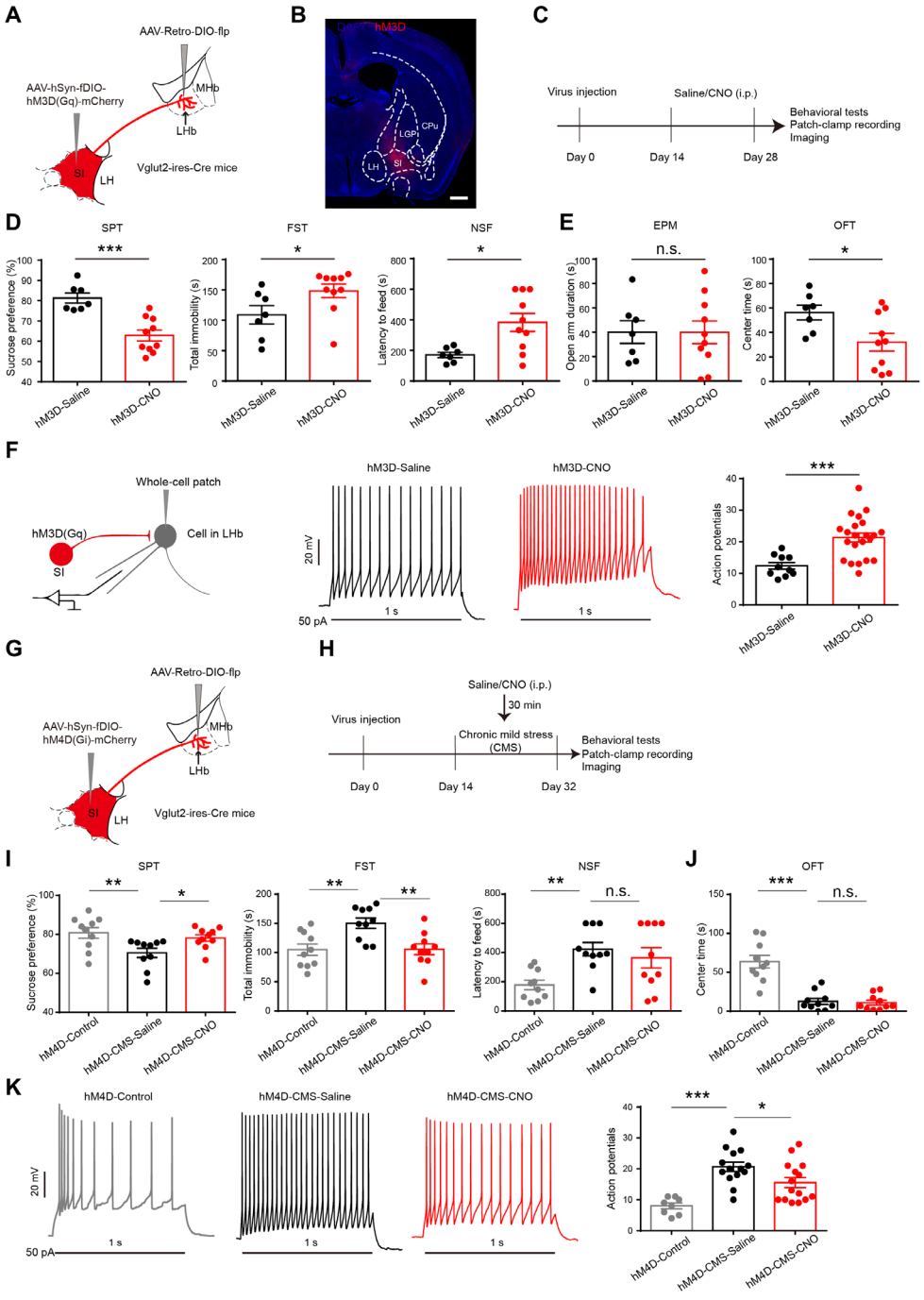

Fig. 4. SI_{VGluT2}-LHb neural circuit modulates depressive- and anxiety-like behaviors. (**A**) Scheme for specific infection of LHb-projecting SI neurons with hM3D in Vglut2-ires-Cre mice. (**B**) Representative image showing the injection site of hM3D virus. Scale bar, 500 μm. (**C**) Schematic of the experimental design. (**D** and **E**) The statistical chart of depressive- and anxiety-like behaviors in three different groups ($n = 7$ to 10 mice per group). Mann-Whitney test, $^{***}P < 0.001$; FST: $^{*}P = 0.02$; NSF: $^{*}P = 0.02$; OFT: $^{*}P = 0.03$. n.s., no significant difference. (**F**) Left: Schematic diagram of patch-clamp recording of the LHb neurons after long-term activation of SI-LHb projections using hM3D. Middle and right: The current-evoked action potentials in LHb neuron of hM3D-Saline and hM3D-CNO mice. Mann-Whitney test, $^{***}P < 0.001$. (**G**) Scheme for specific infection of LHb-projecting SI neurons with hM4D in Vglut2-ires-Cre mice. (**H**) Schematic of the experimental design. The hM4D-control group without AS treatment. Both hM4D-CMS-Saline and hM4D-CMS-CNO groups received AS for 28 days, the hM4D-CMS-Saline group received intraperitoneal saline daily, and the hM4D-CMS-CNO group received intraperitoneal CNO daily for inhibition of the SI_{VGluT2}-LHb neural circuit ($n = 10$ mice per group). (**I** and **J**) The statistical chart of depressive- and anxiety-like behaviors in three different groups. One-way ANOVA with Dunnett's multiple comparisons test: SPT: hM4D-Control versus hM4D-CMS-Saline: $^{**}P = 0.007$ and hM4D-CMS-Saline versus hM4D-CMS-CNO groups: $^{*}P = 0.047$; FST: hM4D-Control versus hM4D-CMS-Saline: $^{**}P = 0.003$ and hM4D-CMS-Saline versus hM4D-CMS-CNO groups: $^{**}P = 0.003$; NSF: hM4D-Control versus hM4D-CMS-Saline: $^{**}P = 0.005$; OFT: hM4D-Control versus hM4D-CMS-Saline: $^{***}P < 0.001$. (**K**) The 50-pA injected current-evoked action potentials in LHb neuron of hM4D-Control, hM4D-CMS-Saline, and hM4D-CMS-CNO mice. One-way ANOVA with Dunnett's multiple comparisons test: hM4D-CMS-Saline versus hM4D-CMS-CNO groups: $^{*}P = 0.03$. Data are means ± SEM.

hM4D-CMS-saline and hM4D-CMS-CNO groups (fig. S9B). The antidepressive effects were also accompanied by significantly reduced excitability in the LHb (Fig. 4K). Thus, SI excitatory inputs can modulate depressive-like phenotype by changing the excitability of LHb neurons. Since the SI_{VGluT2}-LHb neural circuit is very important for the formation of depressive phenotype induced by chronic aversive experience, we further see whether inhibition of the circuit after CMS and before the behavioral tests rescues the depressive-like phenotype. The AAV-Retro-DIO-flp virus was bilaterally injected into the LHb, and AAV-hSyn-fDIO-hM4D-mCherry or AAV-hEF1a-fDIO-mCherry (control virus) was bilaterally injected into the SI of Vglut2-ires-Cre mice (fig. S10A). After 14 days of virus expression, mice were treated with AS for 28 days and then received CNO injection for 7 days to silence the SI_{VGluT2}-LHb neural circuit (fig. S10B). After a series of depressive-related behavioral tests, we observed that the CMS-hM4D-CNO group showed elevated SPT, decreased FST, and decreased tail suspension test (TST) results, compared with the CMS-mCherry-CNO group (fig. S10C). The OFT and EPM tests were not changed (fig. S10D). This indicated that silencing the SI_{VGluT2}-LHb neural circuit after the stress regime would rescue from the depressive-like phenotype.

To specifically manipulate the activity of the postsynaptic LHb neuron targeted by SI glutamatergic neurons, we injected anterograde transsynaptic tracer AAV2/1-hSyn-Cre into the bilateral SI and a Cre-dependent AAV2/9-DIO-hM3Dq-mCherry virus into the LHb of C57 mice (Fig. 5, A and B), which leads to hM3Dq expression in postsynaptic LHb neurons targeted by SI glutamatergic neurons. After 14 days of virus expression, LHb postsynaptic neurons infected with hM3D were activated daily via intraperitoneal injection of CNO lasting for 14 days (Fig. 5C). Then, the mice were subjected to a series of depression- and anxiety-related behavioral tests. We found that chronic activation of LHb neurons innervated by SI significantly induced depressive-like behaviors, but anxiety-like behaviors were not significantly different in both groups (Fig. 5, D and E). Next, we investigated the influence of the inhibition of LHb postsynaptic neurons on depressive/anxiety-like behaviors by delivering AAV2/1-hSyn-Cre into the bilateral SI and Cre-dependent AAV2/9-DIO-hM4Di-mCherry into the LHb (Fig. 5, F and G). After 14 days of virus expression, mice were divided into three groups: the hM4D-CMS-Saline group treated with AS for inducing depressive/anxiety-like behaviors and daily intraperitoneally injected with saline for 28 days, the hM4D-CMS-CNO group treated with the same AS and daily intraperitoneally injected with CNO 30 min before AS to inhibit the activity of LHb postsynaptic neurons, and the hM4D-control group that only went through the same environment as with the CMS group daily (Fig. 5H). After long-term exposure to AS, hM4D-CMS-Saline mice exhibited increased depressive- and anxiety-like behaviors, as tested by the SPT, FST, TST, and OFT, compared with the hM4D-control group (Fig. 5, I and J). Comparing the hM4D-CMS-Saline group with the hM4D-CMS-CNO group, we found that inhibition of the LHb postsynaptic neurons during the chronic stress regime can decrease depressive- and anxiety-like behaviors (Fig. 5, I and J).

Reward consumption buffers depressive-like behaviors induced by activation of the SI_{VGluT2}-LHb circuit

Pieces of evidence have shown that reward can foster stress resilience and promote health across species (*12*, *13*, *49*). The reward can dampen behavioral responses to acute or chronic stress and alleviate negative/depressive emotions (*8*–*11*). In our study, fiber photometry recording showed that reward signals encoded by the SI_{VGluT2}-LHb circuit seemingly suppressed aversive signals (Fig. 1). This prompted us to explore whether reward could buffer chronic activation of SI_{VGluT2}-LHb circuit–induced depressive-like behaviors. We first determined whether reward ameliorated the CMS depression model induced by repeated AS. After repeated AS for 28 days, C57 mice were divided into two groups: the CMS + sucrose group received 5% sucrose intervention; the CMS + water group drinks water freely. The Non-CMS + water group only went through the same environment as with the CMS group and drank water freely daily. Before behavioral testing, we added the 4-hour intervention phase for another 7 days (Fig. 6A). Then, all groups underwent the depressive- and anxiety-like behavioral tests. After long-term exposure to AS, the CMS + water group exhibited increased depressive- and anxiety-like behaviors compared with the Non-CMS + water group (Fig. 6, B and C). Compared with the CMS + water group, sucrose intervention can buffer AS-induced depressive-like behaviors tested in the SPT, FST, and TST but not anxiety behaviors in EPM and OFT (Fig. 6, B and C). To determine whether the sweet taste per se is sufficient to reduce the subsequent response to chronic stress, another group of mice received 4-hour daily exposures to 0.2% saccharin instead of sucrose (fig. S11A). The saccharin-fed group, similar to the sucrose-fed group, had attenuated depressive behavioral responses to CMS (fig. S11B). Meanwhile, we did not observe that saccharin consumption (4 hours/day) for 7 days in intact animals has effects on depressive-like behaviors (fig. S12), suggesting that the rewarding properties of the "desserts" are sufficient to blunt the response of mice to CMS. Next, we explored whether reward could buffer chronic activation of SI_{VGluT2}-LHb circuit–induced depressive-like behaviors. The AAV-Retro-DIO-flp virus was delivered to the LHb of Vglut2-ires-Cre mice, and AAV-hSyn-fDIO-hM3D-mCherry was delivered to the SI (Fig. 6D). After 14 days of virus expression, all mice were induced with depressive-like behaviors by chronic chemogenetic activation of the SI_{VGluT2}-LHb circuit by intraperitoneally injecting CNO for 14 days (Fig. 6E). Then, the mice were divided into three groups: Water, Saline-sucrose, and CNO-sucrose groups. Before behavioral testing, we also added the 4-hour reward intervention phase for another 7 days (Fig. 6E). For the Water group, mice drink water freely; for the Saline-sucrose group, saline is injected into mice daily 30 min before the intervention phase; for the CNO-sucrose group, CNO is injected into mice daily 30 min before the intervention phase for activating the SI_{VGluT2}-LHb circuit. Compared with the Water group, the Saline-sucrose group showed decreased depressive symptoms and decreased excitability of the LHb neurons (Fig. 6, F to H). Animal performance in TST and EPM did not differ significantly (Fig. 6, F and G). This indicated that reward could buffer depressive-like behaviors induced by chronic activation of the SI_{VGluT2}-LHb circuit. Considering that reward consumption inhibited the activity of the SI_{VGluT2}-LHb circuit (Fig. 1), we speculated that the decrease in circuit activity induced by reward consumption may account for the reduced depressive-like behaviors caused by long-term activation of the SI_{VGluT2}-LHb circuit. Comparing the Saline-sucrose group with the CNO-sucrose group, activation of the circuit during the intervention phase could restrain reward antidepressive effects (Fig. 6, F and G). Consistently, the decrease in LHb neuronal excitability in response to reward consumption was also blocked by SI_{VGluT2}-LHb circuit activation (Fig. 6H). This suggested that reward consumption ameliorated depressive-like behaviors through decreasing the activity of the SI_{VGluT2}-LHb circuit.

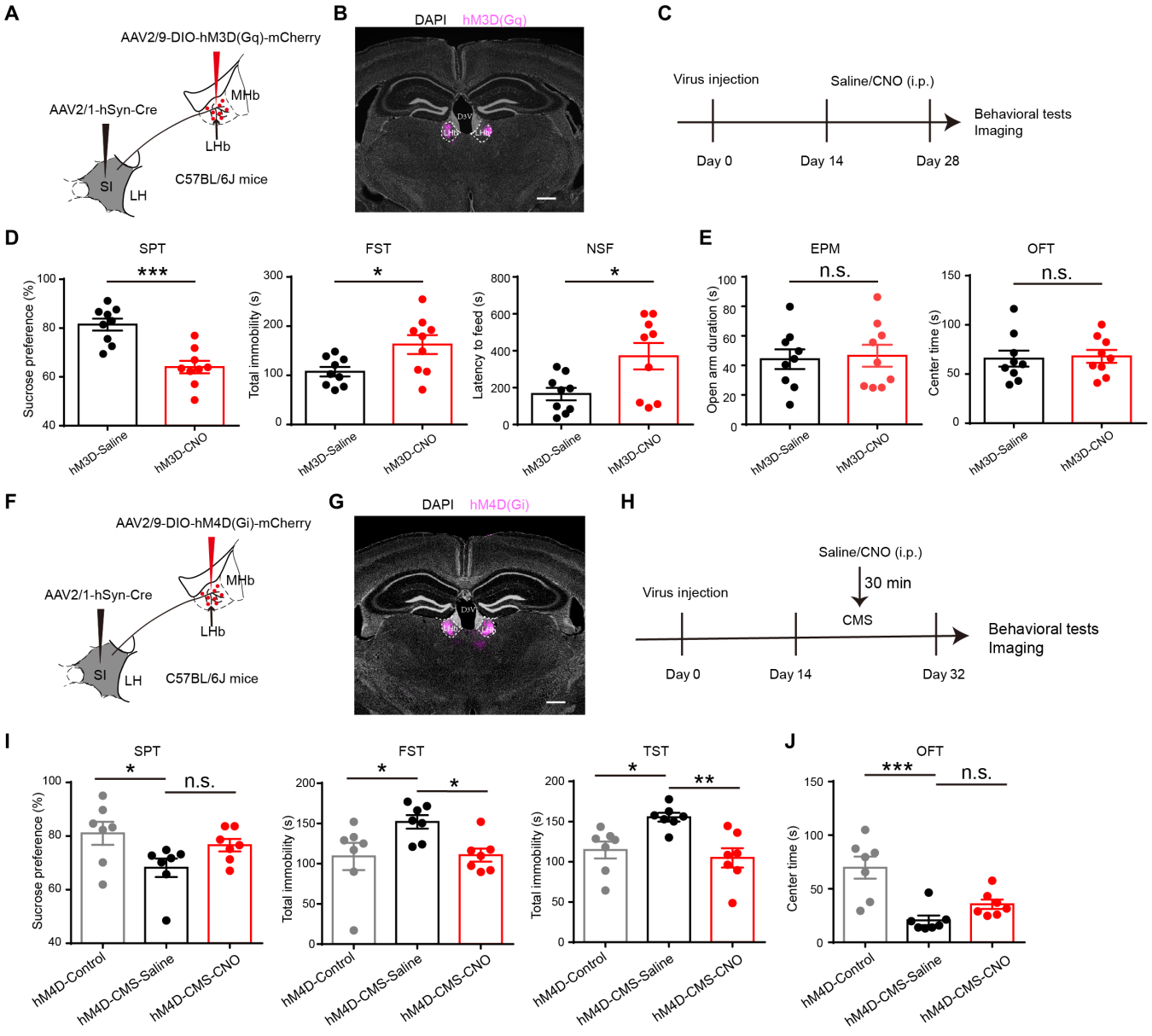

Fig. 5. Chemogenetic manipulation of the LHb postsynaptic neurons regulates depressive-like behaviors. (**A**) Scheme for specific infection of LHb postsynaptic neurons with hM3D. (**B**) Representative image showing LHb postsynaptic neurons with hM3D. Scale bar, 500 μm. (**C**) Schematic of the experimental design. (**D** and **E**) The statistical chart of depressive- and anxiety-like behaviors in mice that received long-term activation of the LHb postsynaptic neurons by CNO and control group that received saline ($n = 9$ animals per group). Mann-Whitney test, SPT: ***$P < 0.001$; FST: *$P = 0.03$; NSF: *$P = 0.04$. Data are means ± SEM. (**F**) Scheme for specific infection of LHb postsynaptic neurons with hM4D. (**G**) Representative image showing LHb postsynaptic neurons with hM4D. Scale bar, 500 μm. (**H**) Schematic of the experimental design. (**I** and **J**) The statistical chart of depressive- and anxiety-like behaviors in three groups ($n = 7$ animals per group). One-way ANOVA with Dunnett's multiple comparisons test: SPT: hM4D-Control versus hM4D-CMS-Saline: *$P = 0.03$; FST: hM4D-Control versus hM4D-CMS-Saline: *$P = 0.04$ and hM4D-CMS-Saline versus hM4D-CMS-CNO groups: *$P = 0.04$; TST: hM4D-Control versus hM4D-CMS-Saline: *$P = 0.02$ and hM4D-CMS-Saline versus hM4D-CMS-CNO groups: **$P = 0.003$; OFT: hM4D-Control versus hM4D-CMS-Saline: ***$P < 0.001$. Data are means ± SEM. DAPI, 4′,6-diamidino-2-phenylindole.

DISCUSSION

Aversive signals urge animals to adjust their behavioral responses in an experience-dependent manner. However, chronic uncontrollable AS can lead to various pathological conditions, including depression (*2*, *3*). Increasing evidence suggests that the LHb is a key brain region in the pathophysiology of depression (*16*, *17*, *19*, *21*). The SI, as a subregion of the BF, is involved in transmitting aversive signals and also projects to LHb (*37*, *39*, *50*). However, whether and how the SI instructs LHb neurons to modulate stress-related behaviors are unknown. In the present study, using fiber photometry, patch-clamp recordings, behavioral tasks, and multichannel recordings, we offer several lines of evidence demonstrating that excitatory projections to the LHb from the SI encode aversive signals and negative reward signals. Reward signals antagonize aversive signals encoded by the SI_{VGluT2}-LHb circuit. Manipulation of the SI_{VGluT2}-LHb circuit using chemogenetics modulates the depressive-like behaviors

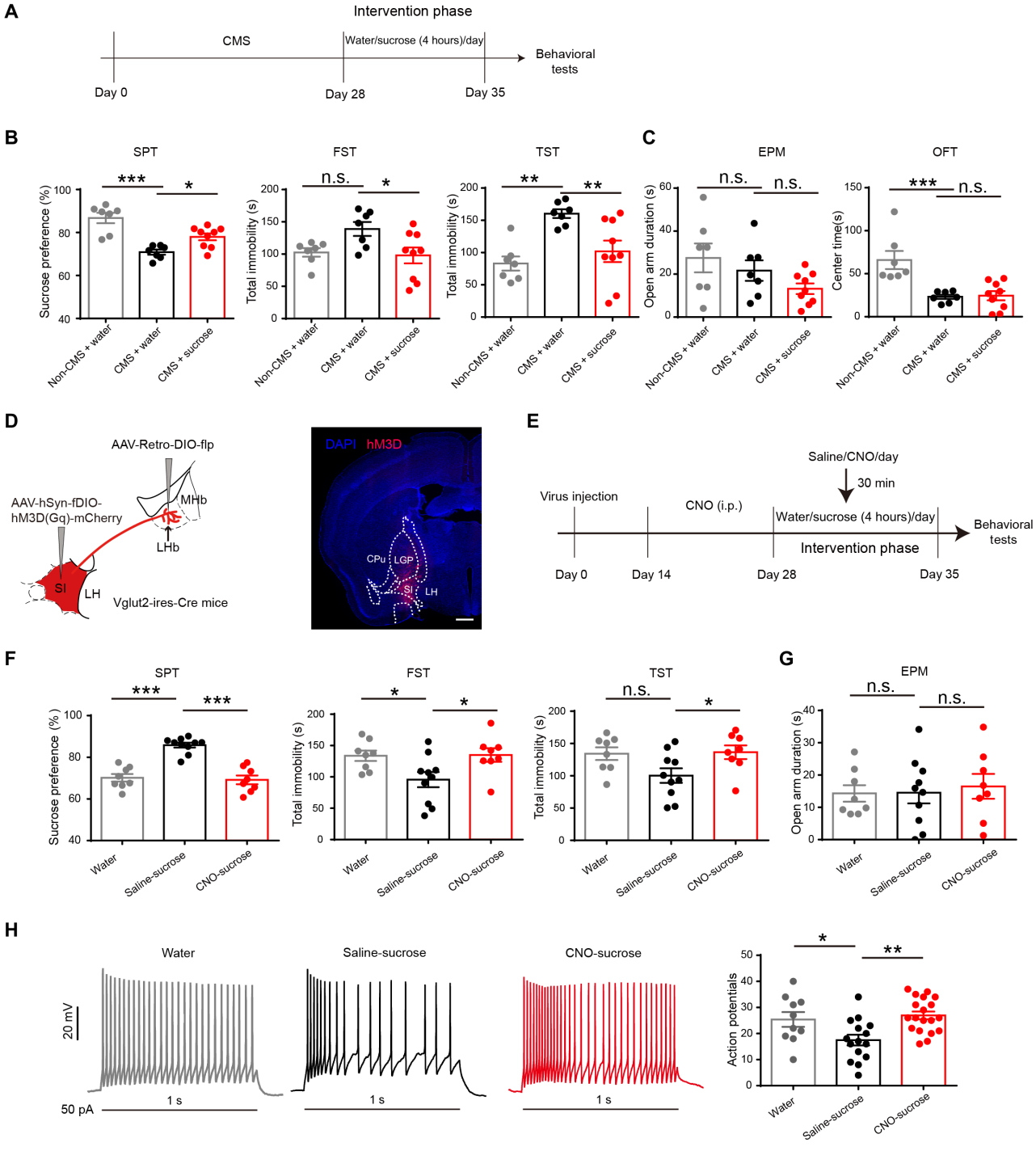

Fig. 6. The reward can buffer depressive-like behaviors induced by activation of the SI_{VGluT2}-LHb neural circuit. (**A**) Schematic of the experimental design. In the 7-day intervention phase, the CMS + sucrose group received 5% sucrose reward for 4 hours daily. (**B** and **C**) The statistical chart of depressive- and anxiety-like behaviors in mice that received long-term exposure to AS. One-way ANOVA with Dunnett's multiple comparisons test, SPT: Non-CMS + water versus CMS + water: ***$P < 0.001$ and CMS + water versus CMS + sucrose: *$P = 0.02$; FST: Non-CMS + water versus CMS + water: $P = 0.06$ and CMS + water versus CMS + sucrose: *$P = 0.02$; TST: Non-CMS + water versus CMS + water: **$P = 0.002$ and CMS + water versus CMS + sucrose: **$P = 0.01$; OFT: Non-CMS + water versus CMS + water: ***$P < 0.001$. Data are means ± SEM. (**D**) Scheme for specific infection of LHb-projecting SI neurons with hM3D in Vglut2-ires-Cre mice. Right: Representative image showing the expression of hM3D virus in the SI. Scale bar, 500 μm. (**E**) Schematic of the experimental design. CNO was injected into mice daily before 30 min for activating the SI_{VGlut2}-LHb pathway before reward was delivered during the intervention phase. (**F** and **G**) The statistical chart of depressive- and anxiety-like behaviors in the three groups. One-way ANOVA with Dunnett's multiple comparisons test, SPT: ***$P < 0.001$; FST: *$P = 0.03$; TST: *$P = 0.04$. Data are means ± SEM. (**H**) The current-evoked action potentials in brain slices of Water-, Saline-sucrose–, and CNO-sucrose–treated mice. One-way ANOVA with Dunnett's multiple comparisons test, Water versus Saline-sucrose: *$P = 0.03$ and Saline-sucrose versus CNO-sucrose: **$P = 0.001$.

accompanying changes in the excitability of LHb neurons. Notably, reward consumption buffers the depressive-like behaviors caused by long-term activation of the SI_{VGluT2}-LHb circuit by antagonizing the circuit activity.

Many studies have revealed that distinct neural populations in the BF have highly convergent inputs and divergent outputs that mediate different behaviors (*39*, *51*, *52*). Both adjacent BF subregions including LPO and VP, which are close to the SI in our study, also project to the LHb region (*37*, *38*, *53*). Previous studies showed that both LPO and VP neurons transmit excitatory signals to LHb, and their influence over LHb predominates over the influence of GABA neurons (*31*, *38*). These LHb-projecting neurons are capable of driving aversive behaviors or even mediating symptoms of depression (*31*, *38*). The SI in our current study also showed a similar phenotype compared with the aforementioned studies. First, with a combination of anterograde viral tracing and patch-clamp recordings, we provided direct evidence that both $VGluT2^+$ and $GABA^+$ neurons in the SI form monosynaptic connections with LHb neurons, but excitatory inputs dominated. Second, activation of the SI_{VGluT2}-LHb circuit, but not the SI_{GABA}-LHb circuit, induced aversive emotion, indicating that SI_{VGluT2} neurons transmit aversive signals to the LHb. Quantification of virus-labeled neurons in the SI, LPO, and VP supports that our study predominantly resides in the SI. However, some minor expression was also observed in the VP and LPO. In addition, unlike the LPO, SI GABAergic projections and glutamatergic projections are concentrated within the lateral aspects of the LHb, but LPO-GABAergic projections are more broadly distributed within the LHb, and the LPO glutamatergic projections are concentrated within the medial aspects of the LHb (*38*). Then, we found that when glutamatergic inputs from the SI were inhibited, most (43.18%) LHb neurons activated by aversive stimuli were also inhibited, suggesting that most aversive responses in the LHb rely on SI excitatory inputs, similar to the hypothalamus-modulating responses of LHb neurons to noxious stimuli (*54*). Considering that lasting aversive stimuli are more likely to cause psychological dysfunction, such as depression, it is reasonable to postulate that long-term activation of the SI, as an upstream region of the LHb, may lead to depressive-like behaviors by transmitting aversive emotions. Optogenetic inhibition or lesion of the LHb inhibits depressive- and anxiety-like behaviors induced by exposure to tail shock or chronic stress (*46*, *51*). In our study, chronic chemogenetic activation of the SI_{VGluT2}-LHb pathway induced depressive-like and other mood-related behaviors, such as anxiety, which mimics long-term exposure to exogenous AS. Inhibition of the pathway significantly decreased long-term AS-induced depressive-like behaviors. Recent studies imply that increased aberrant LHb neuronal activity induced by long-term exposure to AS leads to depressive-like behaviors (*17*, *21*, *47*, *48*). Consistently, we found that both long-term activation of the SI_{VGluT2}-LHb circuit and AS treatment increased excitability of LHb neurons and that inhibition of the SI_{VGluT2}-LHb circuit antagonized the elevated excitability of LHb neurons induced by AS. The latest study has shown that stressful experiences exhibit an AMPA/*N*-methyl-D-aspartate reduction in postsynaptic LHb synapses (*55*), which indicated that the SI glutamatergic inputs might change the synaptic plasticity of LHb neurons, leading to depressive-like behaviors.

Various studies have suggested that the brain's reward system plays a critical role in modulating stress responses (*56*–*60*). A study has shown that reward is an effective way to buffer emotional disorders, such as stress-induced depression (*59*). Food high in fat or sugar, or reward experience, can alleviate negative/depressive emotions and dampen behavioral responses to stress induced by acute or chronic stress (*8*–*11*). In our study, we also observed that long-term stress-induced depressive-like behaviors in mice could be relieved by reward consumption. LHb neurons display inhibition to rewarding events (*14*, *15*). On the basis of fiber photometry evidence, our study suggested that SI-LHb glutamatergic inputs are also inhibited by appetitive stimuli. Previous research has shown that acute stress transforms the responses of LHb reward into punishment-like neural signals (*22*). Notably, in our experiment, reward delivery accompanied by air puff significantly inhibited the increase in GCaMP6m signal induced by the air puff alone. It seems that reward transforms the aversive responses of the LHb into reward signals, indicating that reward consumption can antagonize the effects of stress on the SI_{VGluT2}-LHb circuit. The antagonistic response patterns of the SI_{VGluT2}-LHb pathway to reward and stress drove us to test whether reward could buffer activation of the SI_{VGluT2}-LHb pathway–induced depressive-like behaviors. As expected, reward intervention, such as sucrose/saccharin delivery, ameliorated the depressive behaviors caused by long-term activation of the SI_{VGluT2}-LHb pathway or CMS. When inhibition of the SI_{VGluT2}-LHb circuit using chemogenetics during reward was delivered in the intervention phase, the effects of reward buffering on depressive-like behaviors were greatly reduced, accompanying changes in LHb neuronal excitability. We speculate that the decrease in circuit activity induced by reward consumption may account for the phenomenon of reward consumption ameliorating depressive-like behaviors. However, the possible cellular mechanisms remain to be studied. Besides SI, the LHb neurons also project to the midbrain reward system, such as VTA, which is also a major candidate as a source of negative reward–related signals in dopamine neurons (*14*). It is possible that reward consumption also modulates the activity of the LHb-midbrain circuits, further relieving long-term stress-induced depressive-like behaviors. Anyway, our results confirm that reward can buffer depressive-like behaviors via inhibition of the SI_{VGluT2}-LHb circuit.

Together, we identified the SI-LHb neural circuit as instrumental in modulating depressive-like behaviors by encoding valence signals. Our study indicated that reward relieves stress-induced depressive-like behavior by inhibiting the SI_{VGluT2}-LHb pathway, which may aid the development of new clinical strategies and treatments for neuropsychiatric disorders.

MATERIALS AND METHODS

Animals

The Vglut2-ires-Cre and Vgat-ires-Cre mice (the Jackson Laboratory, stock numbers 028863 and 028862) were purchased from the Jackson Laboratory. C57BL/6J mice were from Beijing HFK Bioscience Co. Ltd. Adult male mice (8 to 16 weeks old) were used and randomly allocated to different groups. Mice were housed under a 12-hour light/dark cycle (7:00 a.m. to 7:00 p.m., lights on) with food and water available ad libitum. All mice were approved by the Jinan University Institutional Animal Care and Use Committee and by the Hubei Provincial Animal Care and Use Committee and complied with the experimental guidelines of the Animal Experimentation Ethics Committee of Huazhong University of Science and Technology, China.

Stereotaxic surgery

AAV-EF1α-DIO-hChR2(H134R)-EYFP and AAV-EF1α-DIO-eArch3.0-EYFP were purchased from the vector core at the University of North Carolina (Chapel Hill, NC, USA). AAV2/1-hSyn-Cre, AAV-hSyn-DIO-EGFP, AAV-CAG-Flex-mCherry, AAV-hEF1α-fDIO-mCherry, AAV-hSyn-fDIO-hM3D(Gq)-mCherry, AAV-CAG-DIO-tasCaspase3, AAV2/9-hSyn-DIO-hM3D(Gq)-mCherry, AAV-hSyn-fDIO-hM3D(Gq)-mCherry, AAV-CAG-ChR2-GFP, AAV-Retro-CAG-DIO-Flp, AAV2/9-hSyn-DIO-hM4D(Gi)-mCherry, and AAV-hSyn-fDIO-hM4D(Gi)-mCherry were purchased from Shanghai Taitool Biological Co. Ltd. (Shanghai, China). AAV-EF1α-DIO-GCaMP6m-WPRE-pA was produced by BrainVTA (Wuhan, China). Mice for virus injection experiments were anesthetized by 10% chloral hydrate in 0.9% NaCl and positioned in a stereotaxic injection frame (Narishige Scientific Instrument Lab, Tokyo, Japan). The virus (200 to 400 nl) was delivered by air pressure application (PMI-100 Pressure Micro Injector, Dagan Ltd) through craniotomy. The injection was performed using the following stereotaxic coordinates for the SI: −0.5 mm from bregma, 1.9 mm lateral from the midline, and 4.8 mm vertical from the cortical surface; for LHb: −1.58 mm from bregma, 0.5 mm lateral from the midline, and 2.8 mm vertical from the cortical surface. The optical fibers for the optogenetic experiments were implanted ~0.5 mm above the LHb. The metal bar for the fixed-head experiments was mounted on the skull using C&B Superbond Quick Cement (Parkell, Brentwood, NY, USA). Behavioral experiments were performed at least 2 weeks after virus injection and at least 1 week after the fibers had been implanted.

fMOST imaging

The VgluT2-ires-Cre mouse was injected unilaterally with AAV-EF1α-DIO-EGFP into the SI region for 2 weeks of expression. Mice were perfused with phosphate-buffered saline (PBS) followed by 4% paraformaldehyde, and brains were postfixed for 24 hours at 4°C. After fixation, the brains were rinsed overnight at 4°C in 0.01 M PBS and subsequently dehydrated in a graded ethanol series (50, 70, and 95%, 1 hour at each concentration) at 4°C. Embedding and sectioning of brain tissue were performed as previously described (*61*). The mosaics of each coronal section were stitched to obtain an entire section based on accurate spatial orientation and neighboring overlap. Raw data were visualized using Amira software (v5.4, FEI, Mérignac Cedex, France).

Fiber photometry recording

Following virus injection into the SI, an optical fiber (230-μm outer diameter, 0.37 numerical aperture; Shanghai Fiblaser Technology Co. Ltd. Shanghai, China) was placed in a ceramic ferrule and inserted ~0.2 mm above the LHb. After surgery, the mice were permitted to recover for at least 1 week. All stimuli including footshock, air puff, sucrose, solid chocolate, and water were delivered and recorded by LabState ver1.0 in the operant behavioral system (AniLab Software & Instruments). The fiber photometry systems (BiolinkOptics, Beijing, China and Thinker Tech, Nanjing, China) were used for recording axon terminal fluorescence signals of the SI projecting to LHb. The laser power at the fiber tip was adjusted to 20 to 30 μW. The fluorescence signals were further low-pass filtered (30-Hz cutoff) at a sampling frequency of 100 Hz. The relative change in fluorescence, $\Delta F/F = (F - F_0)/F_0$, was calculated using F_0 as the baseline fluorescence signal averaged over 4 s before the stimulus. All data were analyzed using MATLAB.

In vivo multichannel recording

Before performing the in vivo multichannel recording experiments, AAV-CAG-DIO-tasCasp3-TEVp was injected into one side of the SI of the VGluT2-ires-Cre mice to ablate VGluT2 neurons, and AAV-EF1a-DIO-eArch3.0-EYFP was injected on the other side to inhibit the activity of the SI-LHb circuit. Two weeks later, a custom-built screw-driven microdrive consisting of a 125-μm optical fiber surrounded by 16 single recording electrodes was implanted into the LHb with ArchT expression in the SI. The electrodes were progressively lowered to the LHb by being moved to a new unit on each recording day. The data recording was acquired by the NeuroPhys System, band-pass filtered at 300 to 6000 Hz, and recorded continuously at 40 kHz. The amplitude threshold for the spike capture was 60 μV. The spikes were manually sorted offline on the basis of principal components analysis 1 (PCA1) and PCA2 using MClust-4.4. The isolation distance (>20) and an L ratio (<0.1) of the individual neurons were selected. To test whether inhibiting the SI excitatory projections modulated LHb neurons in response to aversive stimuli (air puff), we applied a continuous 532-nm laser in 50% of the trials when the air puff (0.5 s) was delivered. A 532-nm laser (Shanghai Dream Lasers Technology Co. Ltd., Shanghai, China) and air puff were controlled by the LabState ver1.0 for operant behavior system (AniLab Software & Instruments Co. Ltd., Ningbo, China). Data analyses were carried out using MATLAB software (MathWorks Inc., Natick, MA, USA). Neurons with a firing rate *Z*-score value >2.2 between 0 and 1 s from the onset of the air puff were considered activated. In computing the firing rate *Z*-score value, mean and SD were defined as the mean and SD during the total recorded time. The spikes of each neuron in the histogram were binned by 50 ms. All mice used in the behavioral experiment were euthanized lastly and checked for virus expression and the position of the implanted fibers or electrodes. To confirm the effect of ablating VGluT2 neurons by AAV-CAG-DIO-tasCasp3-TEVp, a TUNEL (terminal deoxynucleotidyl transferase–mediated deoxyuridine triphosphate nick end labeling) detection kit (no. C1089; Beyotime Biotechnology, Shanghai, China) was used to detect apoptosis.

Real-time place preference assay

The RTPP was performed in the same two-compartment conditioning apparatus (25 cm by 25 cm by 50 cm per chamber). The protocol consisted of two sessions over 2 days. On day 1, a mouse was adapted to the chambers and freely explored the apparatus for 15 min (pretest). On day 2 (RT), one side of the chamber was randomly defined as the conditioning chamber. The 473-nm laser (30 Hz, 10 ms) was delivered once the mouse entered the conditioning chamber. A video-tracking system (ANY-Maze software, Stoelting Co., Wood Dale, IL, USA) recorded all behavioral parameters. Preference or aversion was calculated by dividing the relative time (in percentage) the mouse spent during RT in the conditioning chamber by the relative time (in percentage) the mouse spent in this chamber during the pretest (RT/pretest ratio).

Licking suppression behavior

Head-fixed mice were placed in a sound-attenuated chamber and trained to lick for water. The behavior consists of habituation, conditioning, and test phases. Before habituation, the mice were deprived of water for 2 to 3 days. In the habituation phase, the mice were trained to spontaneously lick water from a tube for 10 min

during two sessions. Each lick triggered the delivery of water (1.5 μl). In the test phase, a 1-s 473-nm laser pulse (30 Hz, 10 ms, 5 to 10 mW) was randomly (5 to 10 s) delivered during mice licking for water. The water, licking, and laser were triggered and recorded by LabState ver1.0 in the operant behavioral system (AniLab Software & Instruments). A lick suppression index was used to quantify the animals' performance as described previously (*44*, *45*)

$$\text{Lick suppression index} = (L_{Pre} - L_{laser})/(L_{Pre} + L_{laser})$$

where L_{Pre} is the number of licks in the 1-s period before laser onset and L_{laser} is the number of licks during the 1-s laser period.

Ex vivo electrophysiology

Ex vivo electrophysiology was carried out as described previously (*7*). For brain slice preparation, mice were deeply anesthetized with isoflurane, and coronal sections (250 μm thick) including the LHb were cut under ice-cold artificial cerebrospinal fluid [ACSF; 119 mM NaCl, 2.5 mM KCl, 1 mM sodium phosphate buffer, 11 mM glucose, 26.2 mM $NaHCO_3$, 2.5 mM $CaCl_2$, and 1.3 mM $MgCl_2$ (at pH 7.4), 290 mOsm] using a vibratome (VT1200S; Leica Microsystems). The brain slices were incubated at 35° ± 1°C for 1 hour and recovered for 1 hour at room temperature in ACSF. A single slice was transferred to the recording chamber and continuously perfused with oxygenated ACSF at a rate of ~2 ml/min. The pipettes, with resistance ranging from 2 to 6 megohms, were filled with intracellular solution containing the following: for voltage clamp: 130 mM $CsMeSO_4$, 10 mM NaCl, 10 mM EGTA, 4 mM MgATP, 0.3 mM Na_3GTP, and 10 mM Hepes, 290 mOsm, adjusted to 7.4 with CsOH; for current clamp: 135 mM $KMeSO_4$, 10 mM KCl, 10 mM Hepes, 10 mM Na_2-phosphocreatine, 4 mM MgATP, and 0.3 mM Na_3GTP, 290 mOsm, adjusted to 7.4 with KOH. Evoked postsynaptic currents were elicited by a 5-ms blue light stimulation of axon terminals of SI projecting to LHb infected with ChR2. EPSCs and IPSCs were recorded when the membrane potential was held at −70 and 0 mV, respectively. To test whether the recorded IPSCs were mediated by GABA receptors, PTX (50 μM) was added to the ACSF. To test whether the recorded EPSCs were mediated by AMPA/kainate receptors, CNQX (10 μM) was added to the ACSF. To examine the monosynaptic nature of PSCs in LHb following light activation of SI inputs, slices were perfused with TTX (1 μM) to block the sodium channel and followed by the addition of 4-AP (100 μM), a potassium channel blocker, to facilitate glutamate release from synaptic terminals. All recordings were performed using a Multiclamp 700B amplifier. Traces were low-pass–filtered at 2 kHz and digitized at 10 kHz. For light stimulation, light pulses were delivered through digital commands from the Digidata 1550A. When stable whole-cell recordings were achieved with an access resistance below 25 megohms, basic electrophysiological properties were recorded. Offline data analysis was performed using Clampfit 10.0 software.

Chronic mild stress model

CMS procedure was carried out as described previously (*7*). The model consists of four different types of stressors: footshock, air puff, fox urine, and physical restraint. The order of stressors was counterbalanced. Mice were individually housed and subjected to four different stressors each day within 28 days. In brief, footshocks (20 times/day, 1 mA, 500 ms) were randomly delivered with intertrial intervals of 15, 20, or 30 s. Air puffs (20 times/day) were randomly delivered to the faces of the mice with intertrial intervals of 10 to 15 s in mice home cages. For fox urine exposure, mice were kept in a transparent plastic container (25 cm by 10 cm by 10 cm, with holes) containing four cotton balls soaked with red fox urine for 30 min/day. For physical restraint, the mice were restrained for 1 hour/day in a plastic restrainer.

Depression-related behavioral test

All behavioral tests were conducted during the light phase (7:00 a.m. to 7:00 p.m.). The order of testing was counterbalanced during behavioral experiments. Anxiety- and depressive-like behaviors were assessed at time points of interest. Behavioral tests were performed within a week, with at least 24-hour intervals between each behavioral test. Depressive-like behaviors were tested in the SPT, FST, NSF, and TST. Anxiety-like behaviors were tested in the EPM and OFT, as previously described (*7*, *62*). For the SPT, mice were tested for preference for a 2% sucrose solution (sucrose, Sigma-Aldrich) using a two-bottle choice procedure. Mice were housed individually for a 2-day test period and were given two bottles, one of sucrose and one of tap water. Every 24 hours, the amounts of sucrose and water consumed were recorded. The positions of the bottles were changed every 24 hours to prevent potential location preference for drinking. The preference for sucrose was determined as the percentage of sucrose solution ingested relative to the total intake. For the FST, during the whole test phase, animal behavior was video-tracked from the side. Mice were placed in a cylinder of water (temperature of 23°C, 20 cm in diameter, 27 cm in height for mice) for 6 min. Immobility was defined as no active movement except that needed to keep the animal from drowning. For the OFT, the open field chamber was made of transparent plastic (50 cm by 50 cm by 40 cm), and a 25 cm by 25 cm center square was color-marked. Mice were placed in the center of a plastic box in a room with dim light and were allowed to explore the arena for 15 min. All animal activity including the time spent in the center area, the total distance, and velocity were recorded for 10 min with an overhead video-tracking system (Med Associates Inc., Fairfax, VT). The box was cleaned with 75% ethanol and dried thoroughly after each test session. For the EPM, the EPM test was used to monitor anxiety-like behavior in mice. The maze apparatus consisted of two opposing open (44 cm by 12 cm) and two enclosed arms (44 cm by 12 cm) extending from a central platform (12 cm by 12 cm). The whole apparatus was elevated 50 cm above the floor. During the test, mice were placed in the center square of the maze, facing an open arm, and were allowed to freely explore the arena during a 6-min test session. A video-tracking system (Ethovision XT software) was used to automatically track and analyze their entries into the open arms and the time they spent in the open arms. The apparatus was wiped clean with 50% ethanol after each trial and dried thoroughly after each test session. For the NSF, food pellets were removed for 24 hours before the test. For testing (T = 10 min), mice were placed in a corner of an unfamiliar white Plexiglas arena (50 cm by 50 cm by 40 cm) with the floor covered in corn cob bedding under bright-light conditions. A single food pellet was placed in the middle of the arena. The latency to eat was measured with a stopwatch and defined on the basis of the first bite of the food pellet. For the TST, each mouse was suspended for 6 min by the tail (2 cm from the end of the tail). The mouse was judged to be immobile when it ceased moving its limbs and body, making only movements that allow itself to breathe.

Quantification and statistical analysis

After the experiment, all mice were euthanized and processed for histological analysis to check for virus expression and positions of the implanted fibers. Only animals with injection sites or fiber placements in the region of interest were included. Quantification and statistical analysis are presented in the figure legends. For quantification of the percentage of virus-infected neurons in different areas (fig. S1), data analysis was performed by hand scoring according to the different brain regions. For axon projection analysis, sections were imaged on the ZEISS LSM 780 using identical microscope settings across all samples. Images were background-subtracted and then binarized on the basis of a pixel intensity threshold that was held constant for all samples analyzed. Regions of interest were then drawn manually with reference to the *Mouse Brain in Stereotaxic Coordinates*, Second Edition, Franklin, K.B.J. and Paxinos, G. Axon density is reported as ((black pixels in the region of interest)/(total pixels in the region of interest)) × 100. For the fiber photometry, data were recorded by the fiber photometry system and analyzed using MATLAB. For the RTPP experiment, data were automatically scored by ANY-Maze software. For licking suppression behavior, data were recorded by LabState ver1.0 in the operant behavioral system. For all depression-related behavioral tests, data are collected on the basis of whether they received different virus injections. Data analysis was performed by an experimenter blind to experimental conditions. The source data are provided as a Source Data file. All statistics were calculated using SPSS software and GraphPad Prism 7 software. Statistical significance was set at $^{*}P < 0.05$, $^{**}P < 0.01$, and $^{***}P < 0.001$.

SUPPLEMENTARY MATERIALS

Supplementary material for this article is available at https://science.org/doi/10.1126/sciadv.abn0193

View/request a protocol for this paper from *Bio-protocol*.

REFERENCES AND NOTES

1. M. Fava, K. S. Kendler, Major depressive disorder. *Neuron* **28**, 335–341 (2000).
2. R. D. Moloney, S. M. O'Mahony, T. G. Dinan, J. F. Cryan, Stress-induced visceral pain: Toward animal models of irritable-bowel syndrome and associated comorbidities. *Front. Psych.* **6**, 15 (2015).
3. C. Menard, M. L. Pfau, G. E. Hodes, V. Kana, V. X. Wang, S. Bouchard, A. Takahashi, M. E. Flanigan, H. Aleyasin, K. B. LeClair, W. G. Janssen, B. Labonte, E. M. Parise, Z. S. Lorsch, S. A. Golden, M. Heshmati, C. Tamminga, G. Turecki, M. Campbell, Z. A. Fayad, C. Y. Tang, M. Merad, S. J. Russo, Social stress induces neurovascular pathology promoting depression. *Nat. Neurosci.* **20**, 1752–1760 (2017).
4. M. L. Wong, J. Licinio, Research and treatment approaches to depression. *Nat. Rev. Neurosci.* **2**, 343–351 (2001).
5. S. J. Rupke, D. Blecke, M. Renfrow, Cognitive therapy for depression. *Am. Fam. Physician* **73**, 83–86 (2006).
6. T. A. LeGates, D. C. Fernandez, S. Hattar, Light as a central modulator of circadian rhythms, sleep and affect. *Nat. Rev. Neurosci.* **15**, 443–454 (2014).
7. L. Huang, Y. Xi, Y. Peng, Y. Yang, X. Huang, Y. Fu, Q. Tao, J. Xiao, T. Yuan, K. An, H. Zhao, M. Pu, F. Xu, T. Xue, M. Luo, K. F. So, C. Ren, A visual circuit related to habenula underlies the antidepressive effects of light therapy. *Neuron* **102**, 128–142.e8 (2019).
8. L. Dube, J. L. LeBel, J. Lu, Affect asymmetry and comfort food consumption. *Physiol. Behav.* **86**, 559–567 (2005).
9. M. C. Wichers, D. Q. Barge-Schaapveld, N. A. Nicolson, F. Peeters, M. de Vries, R. Mengelers, J. van Os, Reduced stress-sensitivity or increased reward experience: The psychological mechanism of response to antidepressant medication. *Neuropsychopharmacology* **34**, 923–931 (2009).
10. Y. M. Ulrich-Lai, A. M. Christiansen, M. M. Ostrander, A. A. Jones, K. R. Jones, D. C. Choi, E. G. Krause, N. K. Evanson, A. R. Furay, J. F. Davis, M. B. Solomon, A. D. de Kloet, K. L. Tamashiro, R. R. Sakai, R. J. Seeley, S. C. Woods, J. P. Herman, Pleasurable behaviors reduce stress via brain reward pathways. *Proc. Natl. Acad. Sci. U.S.A.* **107**, 20529–20534 (2010).
11. S. Dalm, E. R. de Kloet, M. S. Oitzl, Post-training reward partially restores chronic stress induced effects in mice. *PLOS ONE* **7**, e39033 (2012).
12. A. M. Christiansen, A. D. Dekloet, Y. M. Ulrich-Lai, J. P. Herman, "Snacking" causes long term attenuation of HPA axis stress responses and enhancement of brain FosB/deltaFosB expression in rats. *Physiol. Behav.* **103**, 111–116 (2011).
13. Y. Yuan, W. Wu, M. Chen, F. Cai, C. Fan, W. Shen, W. Sun, J. Hu, Reward inhibits paraventricular CRH neurons to relieve stress. *Curr. Biol.* **29**, 1243–1251.e4 (2019).
14. M. Matsumoto, O. Hikosaka, Lateral habenula as a source of negative reward signals in dopamine neurons. *Nature* **447**, 1111–1115 (2007).
15. M. Matsumoto, O. Hikosaka, Representation of negative motivational value in the primate lateral habenula. *Nat. Neurosci.* **12**, 77–84 (2009).
16. B. Li, J. Piriz, M. Mirrione, C. Chung, C. D. Proulx, D. Schulz, F. Henn, R. Malinow, Synaptic potentiation onto habenula neurons in the learned helplessness model of depression. *Nature* **470**, 535–539 (2011).
17. K. Li, T. Zhou, L. Liao, Z. Yang, C. Wong, F. Henn, R. Malinow, J. R. Yates III, H. Hu, βCaMKII in lateral habenula mediates core symptoms of depression. *Science* **341**, 1016–1020 (2013).
18. R. P. Lawson, B. Seymour, E. Loh, A. Lutti, R. J. Dolan, P. Dayan, N. Weiskopf, J. P. Roiser, The habenula encodes negative motivational value associated with primary punishment in humans. *Proc. Natl. Acad. Sci. U.S.A.* **111**, 11858–11863 (2014).
19. C. D. Proulx, O. Hikosaka, R. Malinow, Reward processing by the lateral habenula in normal and depressive behaviors. *Nat. Neurosci.* **17**, 1146–1152 (2014).
20. D. Wang, Y. Li, Q. Feng, Q. Guo, J. Zhou, M. Luo, Learning shapes the aversion and reward responses of lateral habenula neurons. *eLife* **6**, e23045 (2017).
21. Y. Yang, Y. Cui, K. Sang, Y. Dong, Z. Ni, S. Ma, H. Hu, Ketamine blocks bursting in the lateral habenula to rapidly relieve depression. *Nature* **554**, 317–322 (2018).
22. S. J. Shabel, C. Wang, B. Monk, S. Aronson, R. Malinow, Stress transforms lateral habenula reward responses into punishment signals. *Proc. Natl. Acad. Sci. U.S.A.* **116**, 12488–12493 (2019).
23. E. S. Bromberg-Martin, O. Hikosaka, Lateral habenula neurons signal errors in the prediction of reward information. *Nat. Neurosci.* **14**, 1209–1216 (2011).
24. A. Tchenio, S. Lecca, K. Valentinova, M. Mameli, Limiting habenular hyperactivity ameliorates maternal separation-driven depressive-like symptoms. *Nat. Commun.* **8**, 1135 (2017).
25. E. W. Thornton, G. E. Bradbury, Effort and stress influence the effect of lesion of the habenula complex in one-way active avoidance learning. *Physiol. Behav.* **45**, 929–935 (1989).
26. J. Amat, P. D. Sparks, P. Matus-Amat, J. Griggs, L. R. Watkins, S. F. Maier, The role of the habenular complex in the elevation of dorsal raphe nucleus serotonin and the changes in the behavioral responses produced by uncontrollable stress. *Brain Res.* **917**, 118–126 (2001).
27. H. Hu, Y. Cui, Y. Yang, Circuits and functions of the lateral habenula in health and in disease. *Nat. Rev. Neurosci.* **21**, 277–295 (2020).
28. N. Omelchenko, R. Bell, S. R. Sesack, Lateral habenula projections to dopamine and GABA neurons in the rat ventral tegmental area. *Eur. J. Neurosci.* **30**, 1239–1250 (2009).
29. C. Sego, L. Goncalves, L. Lima, I. C. Furigo, J. Donato Jr., M. Metzger, Lateral habenula and the rostromedial tegmental nucleus innervate neurochemically distinct subdivisions of the dorsal raphe nucleus in the rat. *J. Comp. Neurol.* **522**, 1454–1484 (2014).
30. L. Faget, V. Zell, E. Souter, A. McPherson, R. Ressler, N. Gutierrez-Reed, J. H. Yoo, D. Dulcis, T. S. Hnasko, Opponent control of behavioral reinforcement by inhibitory and excitatory projections from the ventral pallidum. *Nat. Commun.* **9**, 849 (2018).
31. D. Knowland, V. Lilascharoen, C. P. Pacia, S. Shin, E. H. Wang, B. K. Lim, Distinct ventral pallidal neural populations mediate separate symptoms of depression. *Cell* **170**, 284–297.e18 (2017).
32. J. Tooley, L. Marconi, J. B. Alipio, B. Matikainen-Ankney, P. Georgiou, A. V. Kravitz, M. C. Creed, Glutamatergic ventral pallidal neurons modulate activity of the habenula-tegmental circuitry and constrain reward seeking. *Biol. Psychiatry* **83**, 1012–1023 (2018).
33. D. S. Zahm, D. H. Root, Review of the cytology and connections of the lateral habenula, an avatar of adaptive behaving. *Pharmacol. Biochem. Behav.* **162**, 3–21 (2017).
34. B. Hangya, S. P. Ranade, M. Lorenc, A. Kepecs, Central cholinergic neurons are rapidly recruited by reinforcement feedback. *Cell* **162**, 1155–1168 (2015).
35. T. C. Harrison, L. Pinto, J. R. Brock, Y. Dan, Calcium imaging of basal forebrain activity during innate and learned behaviors. *Front. Neural. Circuits* **10**, 36 (2016).
36. K. Semba, Multiple output pathways of the basal forebrain: Organization, chemical heterogeneity, and roles in vigilance. *Behav. Brain Res.* **115**, 117–141 (2000).
37. L. Yetnikoff, A. Y. Cheng, H. N. Lavezzi, K. P. Parsley, D. S. Zahm, Sources of input to the rostromedial tegmental nucleus, ventral tegmental area, and lateral habenula compared: A study in rat. *J. Comp. Neurol.* **523**, 2426–2456 (2015).
38. D. J. Barker, J. Miranda-Barrientos, S. Zhang, D. H. Root, H. L. Wang, B. Liu, E. S. Calipari, M. Morales, Lateral preoptic control of the lateral habenula through convergent glutamate and GABA transmission. *Cell Rep.* **21**, 1757–1769 (2017).

39. Y. Cui, G. Lv, S. Jin, J. Peng, J. Yuan, X. He, H. Gong, F. Xu, T. Xu, H. Li, A central amygdala-substantia innominata neural circuitry encodes aversive reinforcement signals. *Cell Rep.* **21**, 1770–1782 (2017).
40. L. Heimer, R. E. Harlan, G. F. Alheid, M. M. Garcia, J. de Olmos, Substantia innominata: A notion which impedes clinical-anatomical correlations in neuropsychiatric disorders. *Neuroscience* **76**, 957–1006 (1997).
41. Z. Gottesfeld, V. J. Massari, E. A. Muth, D. M. Jacobowitz, Stria medullaris: A possible pathway containing GABAergic afferents to the lateral habenula. *Brain Res.* **130**, 184–189 (1977).
42. J. Akerboom, T. W. Chen, T. J. Wardill, L. Tian, J. S. Marvin, S. Mutlu, N. C. Calderon, F. Esposti, B. G. Borghuis, X. R. Sun, A. Gordus, M. B. Orger, R. Portugues, F. Engert, J. J. Macklin, A. Filosa, A. Aggarwal, R. A. Kerr, R. Takagi, S. Kracun, E. Shigetomi, B. S. Khakh, H. Baier, L. Lagnado, S. S. Wang, C. I. Bargmann, B. E. Kimmel, V. Jayaraman, K. Svoboda, D. S. Kim, E. R. Schreiter, L. L. Looger, Optimization of a GCaMP calcium indicator for neural activity imaging. *J. Neurosci.* **32**, 13819–13840 (2012).
43. T. W. Chen, T. J. Wardill, Y. Sun, S. R. Pulver, S. L. Renninger, A. Baohan, E. R. Schreiter, R. A. Kerr, M. B. Orger, V. Jayaraman, L. L. Looger, K. Svoboda, D. S. Kim, Ultrasensitive fluorescent proteins for imaging neuronal activity. *Nature* **499**, 295–300 (2013).
44. J. C. Erlich, D. E. Bush, J. E. Ledoux, The role of the lateral amygdala in the retrieval and maintenance of fear-memories formed by repeated probabilistic reinforcement. *Front. Behav. Neurosci.* **6**, 16 (2012).
45. K. Yu, P. Garcia da Silva, D. F. Albeanu, B. Li, Central amygdala somatostatin neurons gate passive and active defensive behaviors. *J. Neurosci.* **36**, 6488–6496 (2016).
46. L. R. Jacinto, R. Mata, A. Novais, F. Marques, N. Sousa, The habenula as a critical node in chronic stress-related anxiety. *Exp. Neurol.* **289**, 46–54 (2017).
47. R. P. Lawson, C. L. Nord, B. Seymour, D. L. Thomas, P. Dayan, S. Pilling, J. P. Roiser, Disrupted habenula function in major depression. *Mol. Psychiatry* **22**, 202–208 (2017).
48. S. Lecca, A. Pelosi, A. Tchenio, I. Moutkine, R. Lujan, D. Herve, M. Mameli, Rescue of GABAB and GIRK function in the lateral habenula by protein phosphatase 2A inhibition ameliorates depression-like phenotypes in mice. *Nat. Med.* **22**, 254–261 (2016).
49. S. M. Sternson, Hypothalamic survival circuits: Blueprints for purposive behaviors. *Neuron* **77**, 810–824 (2013).
50. Z. Zhu, Q. Ma, L. Miao, H. Yang, L. Pan, K. Li, L. H. Zeng, X. Zhang, J. Wu, S. Hao, S. Lin, X. Ma, W. Mai, X. Feng, Y. Hao, L. Sun, S. Duan, Y. Q. Yu, A substantia innominata-midbrain circuit controls a general aggressive response. *Neuron* **109**, 1540–1553.e9 (2021).
51. S. D. Dolzani, M. V. Baratta, J. Amat, K. L. Agster, M. P. Saddoris, L. R. Watkins, S. F. Maier, Activation of a habenulo-raphe circuit is critical for the behavioral and neurochemical consequences of uncontrollable stress in the male rat. *eNeuro* **3**, ENEURO.0229 (2016).
52. M. Stephenson-Jones, C. Bravo-Rivera, S. Ahrens, A. Furlan, X. Xiao, C. Fernandes-Henriques, B. Li, Opposing contributions of GABAergic and glutamatergic ventral pallidal neurons to motivational behaviors. *Neuron* **105**, 921–933.e5 (2020).
53. D. H. Root, R. I. Melendez, L. Zaborszky, T. C. Napier, The ventral pallidum: Subregion-specific functional anatomy and roles in motivated behaviors. *Prog. Neurobiol.* **130**, 29–70 (2015).
54. S. Lecca, F. J. Meye, M. Trusel, A. Tchenio, J. Harris, M. K. Schwarz, D. Burdakov, F. Georges, M. Mameli, Aversive stimuli drive hypothalamus-to-habenula excitation to promote escape behavior. *eLife* **6**, e30697 (2017).
55. A. Nuno-Perez, M. Trusel, A. L. Lalive, M. Congiu, D. Gastaldo, A. Tchenio, S. Lecca, M. Soiza-Reilly, C. Bagni, M. Mameli, Stress undermines reward-guided cognitive performance through synaptic depression in the lateral habenula. *Neuron* **109**, 947–956.e5 (2021).
56. A. F. Arnsten, Stress signalling pathways that impair prefrontal cortex structure and function. *Nat. Rev. Neurosci.* **10**, 410–422 (2009).
57. M. G. Baxter, E. A. Murray, The amygdala and reward. *Nat. Rev. Neurosci.* **3**, 563–573 (2002).
58. E. E. Belz, J. S. Kennell, R. K. Czambel, R. T. Rubin, M. E. Rhodes, Environmental enrichment lowers stress-responsive hormones in singly housed male and female rats. *Pharmacol. Biochem. Behav.* **76**, 481–486 (2003).
59. J. M. Dutcher, J. D. Creswell, The role of brain reward pathways in stress resilience and health. *Neurosci. Biobehav. Rev.* **95**, 559–567 (2018).
60. D. D. Francis, J. Diorio, P. M. Plotsky, M. J. Meaney, Environmental enrichment reverses the effects of maternal separation on stress reactivity. *J. Neurosci.* **22**, 7840–7843 (2002).
61. Z. Yang, B. Hu, Y. Zhang, Q. Luo, H. Gong, Development of a plastic embedding method for large-volume and fluorescent-protein-expressing tissues. *PLOS ONE* **8**, e60877 (2013).
62. L. Steru, R. Chermat, B. Thierry, P. Simon, The tail suspension test: A new method for screening antidepressants in mice. *Psychopharmacology (Berl)* **85**, 367–370 (1985).

Acknowledgments

Funding: We thank B. Pan for providing a fiber photometry system (Thinker Tech, Nanjing, China). This study was supported by the National Science and Technology Innovation 2030 grant (2021ZD0201002), the National Natural Science Foundation of China (grants 31671105, 31922030, and 31771170), the Science and Technology Program of Guangdong (2018B030334001), and the Science and Technology Program of Guangzhou, China (202007030012). **Author contributions:** H.L. and C.R. designed experiments and supervised the study. Y.C., P.H., and X.X. performed histology, in vivo recording, and some behavioral experiments. X.C. wrote most of the MATLAB code to analyze the data. X.H. and L.H. performed depression- and anxiety-related behavioral experiments and physiological recordings. fMOST was performed by Z.F. and A.L. Y.C. and H.L. wrote the manuscript. **Competing interests:** The authors declare that they have no competing interests. **Data and materials availability:** All data needed to evaluate the conclusions in the paper are present in the paper and/or the Supplementary Materials.

Submitted 29 October 2021
Accepted 23 May 2022
Published 8 July 2022
10.1126/sciadv.abn0193